

Application potential of coarse-grained diamond grinding wheels for precision grinding of optical materials

Ekkard Brinksmeier¹ · Oltmann Riemer¹ · Kai Rickens¹ · Daniel Berger¹ 

Received: 1 June 2016 / Accepted: 13 September 2016 / Published online: 26 September 2016
© German Academic Society for Production Engineering (WGP) 2016

Abstract Fine-grained resin bonded diamond tools are often used for ultra-precision machining of brittle materials to achieve optical surfaces. A well-known drawback is the high tool wear. Therefore, grinding processes need to be developed exhibiting less wear and higher profitability. Consequently, the presented work focuses on conditioning a mono-layered, coarse-grained diamond grinding wheel with a spherical profile and an average grain size of 301 μm by combining a thermo-chemical and a mechanical-abrasive dressing technique. This processing leads to a run-out error of the grinding wheel in a low-micrometer range. Additionally, the thermo-chemical dressing leads to flattened grains, which supports the generation of hydrostatic pressure in the cutting zone and enables ductile-mode grinding of hard and brittle materials. After dressing, the application characteristics of coarse-grained diamond grinding wheels were examined by grinding optical glasses, fused silica and glass-ceramics in two different kinematics, plunge-cut surface grinding and cross grinding. For plunge-cut surface grinding, a critical depth of cut and surface roughness were determined and for cross-grinding experiments the subsurface damage was analyzed additionally. Finally, the identified parameters for ductile-machining with coarse-grained diamond grinding wheels were used for grinding a surface of 2000 mm^2 in glass-ceramics.

Keywords Ultra-precision grinding · Coarse grains · Subsurface damage · Optical materials

1 Introduction

For the machining of hard and brittle materials like ceramics, carbides and optical glasses, ultra-precision grinding is a key technology. The demand for high precision functional components for automotive, communication and electronics industry increases constantly. Hence, economical and qualitative aspects become more important [1]. The main objective is the manufacturing of components with form accuracies in the submicron-range, surface roughness of a few nanometers and a damage-free surface layer zone. These characteristic features for ultra-precision grinding should be reached, if possible, in one single machining step. Therefore, fine-grained, resin bonded tools are used in order to achieve high surface qualities by machining below the critical or minimum uncut chip thickness, maintaining a ductile-regime grinding process [2–4]. Nevertheless, these tools exhibit a high tool wear, and in consequence several dressing processes during the manufacturing of optical components are necessary [5]. Dressing is ranked among the auxiliary processes, and the associated time should be as short as possible, as it deteriorates the economic aspects of a manufacturing process. However, without dressing, form accuracy and surface quality are decreasing.

One approach to overcome these drawbacks and to avoid high tool wear is the application of coarse-grained diamond grinding wheels, so-called engineered grinding wheels. These tools are dressed only once before grinding and remain in a suitable condition for ultra-precision grinding for a long time. With respect to the required condition of the coarse grains for ultra-precision grinding, they are flattened in order to achieve a hydrostatic pressure in the contact zone, supporting ductile-regime grinding mechanisms. Previous research has shown the ability of

✉ Daniel Berger
d.berger@lfm.uni-bremen.de;
<http://www.lfm.uni-bremen.de>

¹ Laboratory for Precision Machining (LFM), University of Bremen, Badgasteiner Str. 2, 28359 Bremen, Germany

these tools for grinding hard and brittle materials. Rickens et al. [6] and Zhao et al. [7] performed a mechanical-abrasive precision conditioning process, where the grains are dressed by a rotating dressing tool, until the height level of the metallic bond is reached. Thereafter, the bond is set back by ELID (Electrolytic In-Process Dressing) and as a result the flattened grains are exposed. Due to the fact that all grains are flattened down to the height level of the metallic bond, a similar protrusion height within a range of 2.5 μm was achieved. A uniform envelope curve was obtained including a low run-out error, which is an essential prerequisite for ultra-precision grinding.

Bing et al. [8] found that a micro-structuring of coarse-grained diamond wheels by laser leads to lower subsurface damage, but unfortunately to higher surface roughness than in dressing techniques without micro-structuring. The laser cuts the protruding grains and structures the grinding wheel topography, but it can neither affect the envelope nor reduce the run-out error.

The disadvantage of the mechanical abrasive dressing technique is the time-intensive dressing process which leads to increasing auxiliary process times again.

Therefore, a thermo-chemical dressing process has been developed recently. This process is based on dynamic friction polishing, using the friction between grinding wheel and austenitic chrome nickel steel calottes [9].

In this paper, for the first time a combination of both dressing techniques, thermo-chemical and mechanical-abrasive dressing, is realized for generating a grinding wheel topography which is useful for ultra-precision grinding in a shorter time period than the former mechanical-abrasive dressing process. The conditioned grinding wheel is applied for grinding experiments on optical glasses BK7 and SF57, fused silica (SQ1) and the glass-ceramic Zerodur[®]. Two grinding strategies, plunge-cut surface grinding and cross grinding, are performed. In both grinding strategies, the depth of cut is increased during the grinding process. Plunge-cut surface grinding allows the determination of a critical depth of cut for the different materials. Surface roughness is measured in the ductile-machined areas of the ground grooves. Besides the surface roughness, the subsurface damage is determined in cross grinding experiments. The results show that engineered grinding wheels can overcome the issue of tool wear by maintaining a surface roughness in a low nanometer range and subsurface damage in a low micrometer range.

2 Characteristics and dressing of engineered grinding wheels

Engineered grinding wheels exhibit a deterministic macro and micro topography. Thus, these tools are geometrically and topographically definable, exhibiting a uniform

protrusion height of the abrasive grains for a closely tolerated uncut chip thickness, which should be below the material dependent critical uncut chip thickness [10]. This is achieved by flattening the coarse diamond grains, which facilitates a hydrostatic pressure in the contact zone, supporting ductile-regime grinding [11].

Table 1 shows the specification of the engineered grinding wheel used in this study. The applied grinding wheel's body is made from high-alloyed austenitic steel and is manufactured by precision turning. The wheel's body incorporates a co-axial reference cylinder for ensuring a run-out error smaller than 2 μm of the body itself and in order to maintain low unbalances. The diamond grains are bonded by an electroplating process, arranging the diamond grains in a single layer. Due to the coarse grains and the hard bond, the tools exhibit a high wear resistance.

Figure 1 shows the requirements on the dressing process (a) and the set-up for thermo-chemical dressing of engineered grinding wheels (b). The process itself is characterized by two rotating austenitic steel calottes, mounted on two linear slides and driven by geared motors and pressed against the grinding wheel with a specific force $F_d = 5 \text{ N}$. The force is applied from two sides in order to avoid torque to the grinding wheel. The calottes are rotating at $n_{ca} = 250 \text{ min}^{-1}$, while the engineered grinding wheel has a rotational speed of $v_{cd} = 20 \text{ m/s}$. The dressing process lasts for 180 min and is monitored by an acoustic emission sensor, maintaining a uniform dressing process.

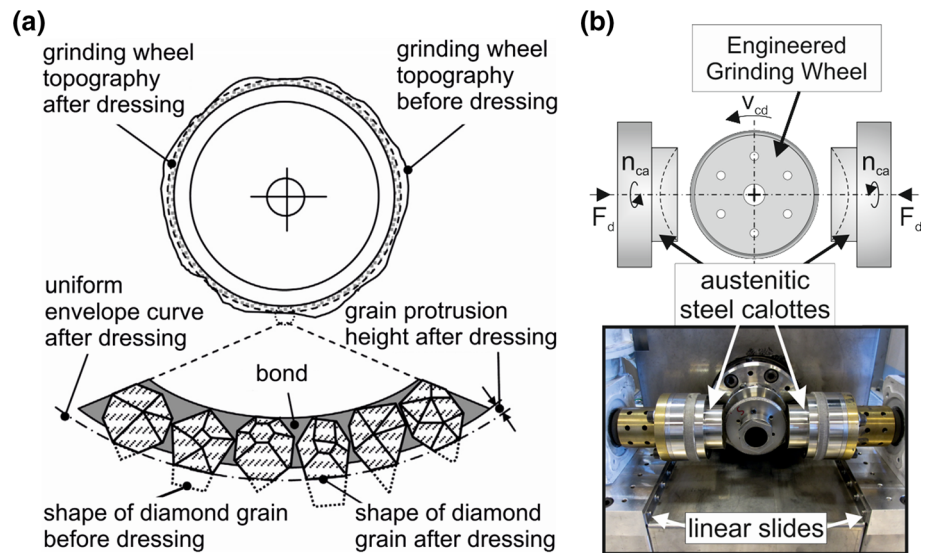
The thermo-chemical dressing technique is based on diamond friction polishing, underlying three main wear mechanisms. Primarily, the friction between the steel calottes and the diamond abrasive grains of the grinding wheel leads to a thermo-chemical reaction between the carbon atoms of the diamond and the oxygen in the experimental environment, building carbon dioxide at temperatures between 600 and 800 $^{\circ}\text{C}$.

Secondarily, catalyzing elements within the austenitic steel calottes, like chrome and nickel, reduce the graphitization temperature of diamond down to 600 $^{\circ}\text{C}$ [12]. As a third wear mechanism, the diffusion of carbon atoms from

Table 1 Specifications of the engineered grinding wheel

Wheel specification	Values
Average grain size d_G	301 μm (D301)
Concentration	C100, single-layered
Bond	Electroplated
Diameter d_s	75 mm
Width b_s	3.5 mm
Profile	Spherical (radius 37.5 mm)
Number of active grits on wheel's circumference (thereof flattened)	750 (150)

Fig. 1 Engineered wheel with coarse grains to be flattened (a) and thermo-chemical dressing process (b)



diamond into the austenitic steel is assumed in literature [13]. Unfortunately, it is not possible to reach a similar protrusion height for all diamond grains by thermo-chemical dressing due to the limited precision of the dressing process, leading to a run-out error of about 18 μm . The remaining run-out error results from the geometric shape of the natural diamond grains, which is subject to a strong variation. The emerging envelope curve is characterized by the difference between the highest and the lowest protruding diamond grain. Only the diamond grains protruding high enough get in contact with the dressing tool, while some diamond grains never do. The generated plateaus of the flattened grains at some point decelerate a further thermo-chemical wear, due to the larger surface contacting with the steel of the dressing tool.

Hence, a subsequent dressing process has to be performed on the grinding machine tool with a diamond coated steel calotte (D46) to lower the run-out error by a mechanical-abrasive ablation. The diamond-coated calotte and the engineered grinding wheel are rotating with the same speeds like in the thermo-chemical dressing process. The calculation of the common dressing parameters, like q_{ed} and U_d , are not appropriate for this dressing process, because the rotational direction of grinding and dressing tool are oriented orthogonal to each other. Moreover, there is no feed per revolution, as the dressing depth of cut a_{ed} , which is presented in Fig. 2, was increased irregularly. Within the machine tool, a dynamometer (Kistler Type 9254) is integrated for monitoring normal, tangential and feed forces during the mechanical-abrasive dressing process. Figure 2 shows that a force-controlled mechanical-abrasive dressing process finally leads to a lower run-out error (7 μm) than a path-controlled (12 μm , the error bars are resulting from multiple measurements). This results from the asymmetric dressing process on the machine tool. The effective normal force of 8 N during the path-controlled process (Fig. 2 left)

causes a torque. This leads to an ellipsoidal envelope curve and consequentially to larger deviations among the protrusion heights of the flattened diamond grains. The thermo-chemical and mechanical-abrasive dressing process have both been carried out only once before the grinding experiments, as the coarse diamond grains offer very low grain wear, which was investigated in former experiments [14].

Only a fraction of the bonded diamond grains were flattened with the thermo-chemical dressing technique and were in contact with the workpiece during the grinding process. The amount of flattened diamond grains was determined by digital microscopy (Digital Camera Leica DVM 2500, Objective lens VZ750C). The entire wheel topography was investigated by rotating the grinding wheel under the objective lens. There are about 150 grains on the D301-tool around the whole wheel circumference of 236 mm (theoretical maximum for this grain size is approx. 750 grains) which have been visibly dressed and are in contact with the dressing tool, while the other grains are not protruding high enough (Table 1).

3 Experimental setup

The grinding experiments were performed on a 5-axis ultra-precision grinding machine tool (Nanotech 500FG). The lubricant (8 % emulsion with FRIGOMET GB 477, a coolant especially designed for grinding of optical glass) was supplied by a round nozzle. For investigating the grinding performance of engineered grinding wheels (Table 1), which were dressed as described in chapter 2, two grinding strategies, plunge-cut and cross grinding, on four different hard-to-machine optical workpiece materials (Table 2) were used in the experiments. The plunge-cut grinding experiments were replicated once. The cross-grinding experiments were performed without a replication due to high set-up times.

Fig. 2 Measured run-out error of D301 grinding wheel while mechanical-abrasive dressing

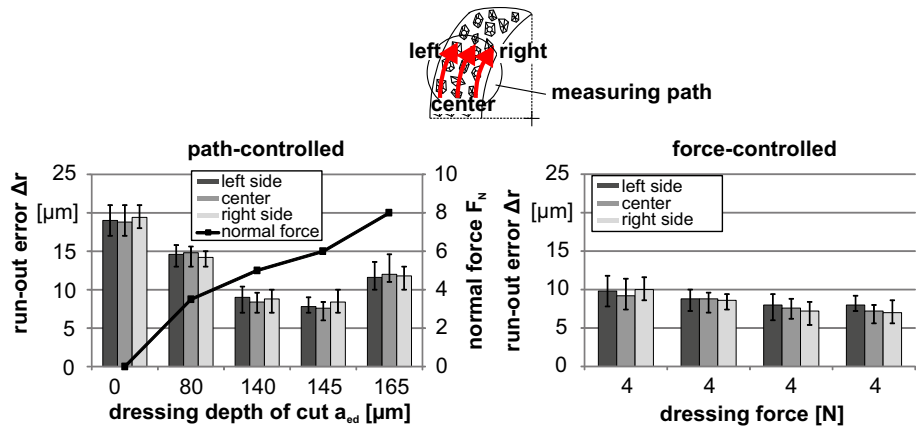


Table 2 Properties of machined materials

Material	Measured values			Calculated
	Vickers hardness	Young’s modulus	Critical stress intensity factor	Critical uncut chip thickness
	H (GPa)	E (GPa)	K _c (MPam ^{1/2})	h _{cu,crit} (nm)
SF57	6.4	100	0.75	32
Zerodur [®]	7.2	94	1.14	50
BK7	6.4	86	0.97	47
SQ1	6.1	74	0.9	40

SF57 is a dense flint glass, consisting of 70–80 % lead(II) oxide and 20–30 % silicon dioxide. It is mainly used for oculars or camera objectives [15]. BK7 is a borosilicate crown glass, utilized for the manufacturing of optical lenses, prisms or mirrors for objectives or microscopes. It consists of 70 % silicon dioxide and in equal parts (approx. 10 %) of sodium oxide, potassium oxide and boron trioxide [16]. The fused silica SQ1 exclusively consists of silicon dioxide and is applied as a window- and lens-material in different applications due to its very large wavelength transmittance range (230–3500 nm) [17]. Zerodur[®], an aluminosilicate glass-ceramic, exhibits a crystalline residual phase, caused by the aluminum oxide which is the main component (approx. 25 %) besides the silicon dioxide (approx. 55 %). The material is applied in space technology, for example as a substrate material for mirrors in modern large telescopes, due to its low coefficient of thermal expansion (CTE) [18].

The material dependent critical uncut chip thickness depends on Vickers hardness H, Young’s modulus E and critical stress intensity factor K_c and is calculated after Bifano et al. by Eq. 1 [2]. The values for h_{cu,crit} for the four different materials are listed in Table 2.

$$h_{cu,crit} = 0.15 \left(\frac{E}{H} \right) \left(\frac{K_c}{H} \right)^2 \tag{1}$$

After plunge-cut grinding experiments, the critical depth of cut and surface roughness were determined. Both were analyzed by white light interferometry. For the

determination of surface roughness, a lens with a magnification of 50× was applied. The detected area was 0.335 × 0.335 mm and was analyzed by applying a global leveling and a cutoff λ = 0.08 mm for filtering the data. This procedure was also performed for analyzing the depth of cut, but with a lens with 10x magnification (area 1.66 mm × 1.66 mm). In order to analyze the subsurface damage after cross grinding experiments, the boundary layer of the ground surface was partially removed, followed by an etching process to make micro cracks visible.

4 Grinding strategies and results

4.1 Plunge-cut surface grinding with different depths of cut

The identification of the parameters for ductile-mode grinding of optical glasses and glass ceramics with engineered grinding wheels is important to understand the material removal mechanisms. In order to find the optimum parameters for achieving this, plunge-cut surface grinding experiments are carried out. While cutting speed v_c and feed rate v_f are constant during one grinding path, the depth of cut a_c is varied by moving the tool into the workpiece in z-direction (taper grinding, Fig. 3). It is known that a critical depth of cut a_{c,crit} exists, where a transition from ductile to brittle machining takes place. The aim of the experiments

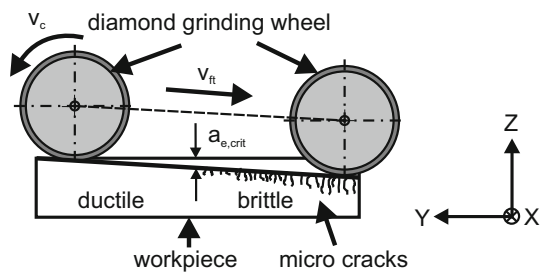


Fig. 3 Plunge-cut surface grinding with increasing depth of cut a_e during grinding experiment

Table 3 Grinding parameters for plunge-cut surface grinding

Workpiece materials	SF57, Zerodur [®] , BK7, SQ1
Feed rate v_f (mm/min)	3, 10
Cutting speed v_c (m/s)	10, 30
Depth of cut a_e (μm)	0–7, constantly increasing on a length of 20 mm ($\alpha = 0.02^\circ$)

is to determine the critical depth of cut for the machined materials at different cutting speeds and feed rates. Table 3 shows the grinding parameters of the experiments on optical materials BK7, SF57, SQ1 and Zerodur[®].

4.1.1 Critical depth of cut

The transition point from ductile to brittle machining can be detected as shown in Fig. 4. Ductile machining abruptly turns to a brittle behavior of the material, leading to large fractures, thus to high surface roughness. The point of transition, corresponding to the critical depth of cut $a_{e,crit}$, is characterized in Fig. 4 left. The brittle behavior causes a larger depth of the groove (Fig. 4 right). The visible

discrepancies according to the groove depth are an indicator for brittle material behavior. The measured topography exhibits parts with far deeper scratches (deep blue parts according to the color scale, >400 nm) than on ductile machined areas. The horizontal profile sections in Fig. 4 seem to be at the same position, yet the profile section in the lower picture is set only a few μm in feed direction, but as the profiles show, the groove depth is much higher than on the upper profile section. This can only be derived from brittle material behavior.

The values for critical depth of cut $a_{e,crit}$ for the different materials are presented in Fig. 5. These values are not the theoretical values of the machined materials, but the measured values on the transition point from ductile to brittle behavior which was determined as described in Fig. 4. Obviously, dependence from cutting speed or feed rate can be hardly identified due to a strong variation of the measured values. Also, a differentiation between the individual materials is difficult. It could be stated that SF57 reveals the highest critical depths of cut, but that there is almost no influence of the machining parameters. Zerodur[®] and SQ1 show the lowest overall values, while SQ1 should be machined with high cutting speeds (30 m/s) and high feed rates (10 mm/min) and Zerodur[®] with high cutting speeds (30 m/s) but low feed rates (3 mm/min). BK7 offers the highest critical depth of cut at low cutting speeds and low feed rates. The error bars result from the replicated grinding experiments. In conclusion, it must be stated that all materials exhibit quite low critical depths of cut, as they range between 0.2 and 0.5 μm . Regarding Fig. 4, the brittle fracture amounts only a small proportion of the ground groove (approx. 10 %) and is obviously caused by one certain point on a specific diamond grain. Thus, the relation between the critical chip thickness and the critical depth of

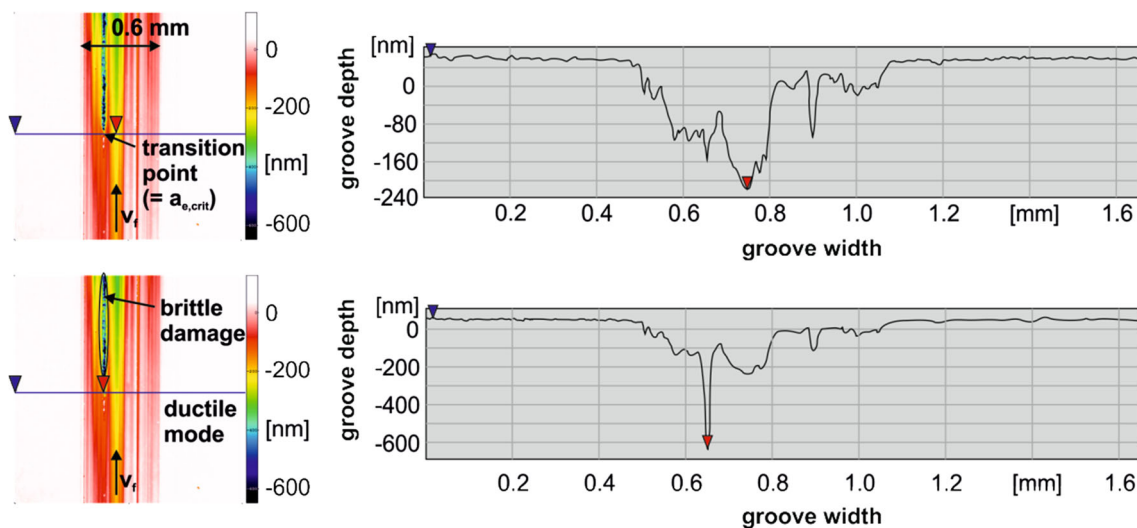


Fig. 4 Detection of transition point from ductile to brittle material behavior, where critical depth of cut $a_{e,crit}$ is determined

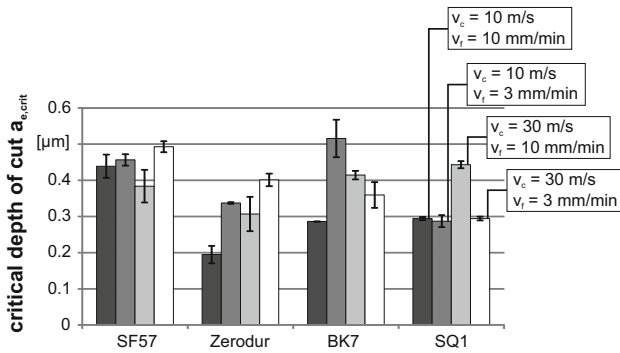


Fig. 5 Critical depth of cut $a_{e,crit}$ for SF57, Zerodur®, BK7 and SQ1, depending on cutting speed v_c and feed rate v_f

cut has a minor influence and $a_{e,crit}$ is characterized mainly by the topography of the tool’s abrasive layer. Equation (2) explains the relation between the uncut chip thickness h_{cu} and the grain shape connected with the grinding wheel topography, characterized by the parameter z_e .

$$h_{cu} = \left(\frac{1}{c_2 + 1} \right)^{\frac{1}{c_2}} \cdot z_e \quad (2)$$

The grain shape is characterized by c_1 and c_2 . It is not explained in detail here, because the grain shape was not varied during the grinding experiments. The parameter z_e is the ratio between the number of active grits N_{GA} and grit density N_{GV} . As only 20 % of the grits are active during grinding, the maximum uncut chip thickness decreases and is strongly influenced by the topography of the abrasive layer. This leads to an exceedance of the critical uncut chip thickness at low depths of cut, as shown in Eq. (3).

$$a_e = \frac{(h_{cu} \cdot v_c)^2}{(4\pi^2 \cdot v_f^2 \cdot d_s)} \quad (3)$$

Connected with Eq. (2), this means that a decreasing uncut chip thickness leads to a decreasing depth of cut.

4.1.2 Surface roughness

In order to prove the possibility to machine hard and brittle materials with engineered grinding wheels, surface roughness S_a is determined in the ductile area, before the transition from ductile to brittle machining appears. Results for S_a are shown in Fig. 6. The best surface quality is obtained for SQ1 for all process parameters; S_a -values are between 4 nm (minimum value) and 17 nm (maximum value). The roughness values for BK7 (7–33 nm), SF57 (5–25 nm) and Zerodur® (6–32 nm) are characterized by a stronger variation. In general, BK7 and Zerodur® exhibit the highest roughness values, followed by SF57 and, as already mentioned, SQ1. Nevertheless, it may be stated that all materials are suitable for ductile machining with engineered grinding

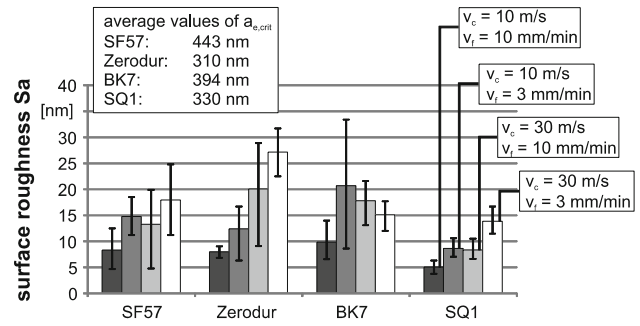


Fig. 6 Surface roughness S_a of ground surfaces by plunge-cut surface grinding at transition point between ductile and brittle machining

wheels regarding surface quality, as the results exhibit roughness values <35 nm. Besides, it is remarkable that the lowest values of surface roughness are determined for a low cutting speed (10 m/s) and a high feed rate (10 mm/min) for all materials, but still a precise statement on the influences of cutting speed and feed rate is not obvious due to a partially strong variation as shown by larger error bars, which were calculated out of multiple measurements.

4.2 Cross grinding with different depths of cut

Surface grinding experiments with rotating workpiece are conducted in cross grinding mode, as Sun et al. [19] found that this kinematics generates more homogeneous surfaces than parallel grinding. In order to find the critical depth of cut for cross surface grinding, the workpiece is tilted by an angle of 0.006° , leading to a variation of depth of cut from $a_{e,max} = 8 \mu m$ to $a_{e,min} < 1 \mu m$, as shown in Fig. 7. For this kinematics, the parameters in Table 4 are set. Cutting speed and feed rate were adopted from former grinding experiments.

The variation of depth of cut across the ground surface leads to an area where brittle fracture is predominant (area #1), a transition area between brittle and ductile material removal mechanism (#2) and an area where only ductile-regime grinding is predominant (#3). On every workpiece, an area with the initial polished surface remains (#4) in order to be able to detect the end of the ground surface. Surface roughness S_a and subsurface damage are evaluated at the different areas on the ground surface (Fig. 8). It is obvious that brittle fracture is predominant on the left side of the workpiece, caused by depths of cut $a_e > 3 \mu m$. For this reason, only the areas machined with depths of cut $a_e \leq 3 \mu m$ are investigated here.

4.2.1 Surface roughness

Figure 9 reveals the surface quality of cross ground surfaces at different measurement locations. The error bars are

Fig. 7 Kinematics of cross grinding experiments with tilted workpiece

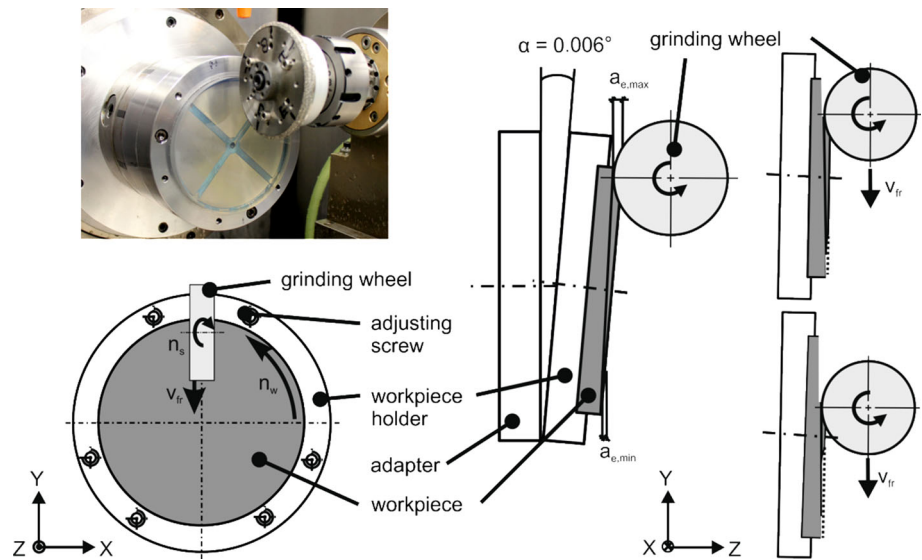


Table 4 Grinding parameters for cross grinding

Workpiece materials	BK7, SF57, SQ1, Zerodur®
Feed rate v_f (mm/min)	3
Cutting speed v_c (m/s)	30
Workpiece rotation n_w (min^{-1})	150
Inclination angle	0.006° (z : $0.09 \mu\text{m/y}$; 1 mm)
Depth of cut a_e (μm)	0–8, constantly increasing

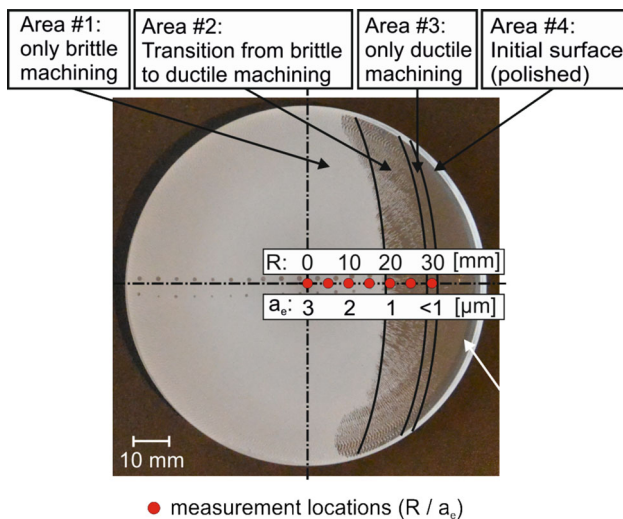


Fig. 8 Measurement locations for determining surface roughness and subsurface damage of cross grinding experiments

derived from multiple measurements and represent the minimum and maximum value. It is notable that SQ1 reveals the lowest S_a -values, as even at a depth of cut of $a_e = 3 \mu\text{m}$ the surface roughness is below $0.2 \mu\text{m}$. It shows

a declining trend, so that at a radial distance of 30 mm a roughness of $S_a = 19 \text{ nm}$ is measured.

For SF57 the surface roughness S_a drops below $0.2 \mu\text{m}$ at $a_e = 0.5 \mu\text{m}$, while the S_a -values have been between 0.5 and $0.8 \mu\text{m}$ before, which shows that if this material is machined above $h_{\text{cu,crit}}$ (SF57 has the lowest value compared to the other machined materials), brittle damage resulting in a rugged surface is the case. But, when the chip thickness falls below $h_{\text{cu,crit}}$, SF57 can be machined at a very low surface roughness, as the surface topography in Fig. 9 proves ($S_a = 13 \text{ nm}$). The transition between brittle and ductile machining appears much smoother for the other materials. SQ1 exhibits the best surface quality with roughness values below $0.1 \mu\text{m}$ over a wide range of depths of cut, which has already been observed in plunge-cut surface grinding experiments. Ductile machining of BK7 and Zerodur® is only possible with depths of cut below $1 \mu\text{m}$ using engineered grinding wheels. At a radial distance of 30 mm, the depth of cut is below $0.5 \mu\text{m}$, enabling the ductile machining of SF57, Zerodur®, BK7 and SQ1. Roughness values of 13 nm (SF57), 28 nm (Zerodur®), 17 nm (BK7) and 19 nm (SQ1), respectively, were detected.

4.2.2 Subsurface damage

The subsurface damage is determined by polishing a calotte into the ground surfaces by using a rotating steel ball (radius $R_{\text{ba}} = 15 \text{ mm}$) and a polishing paste with a diamond grain size of $1 \mu\text{m}$. Subsequently, the polished workpieces are etched for 5 min in 1 % hydrofluoric acid to expose the subsurface damage. The subsurface damage is determined by the procedure presented in Fig. 10.

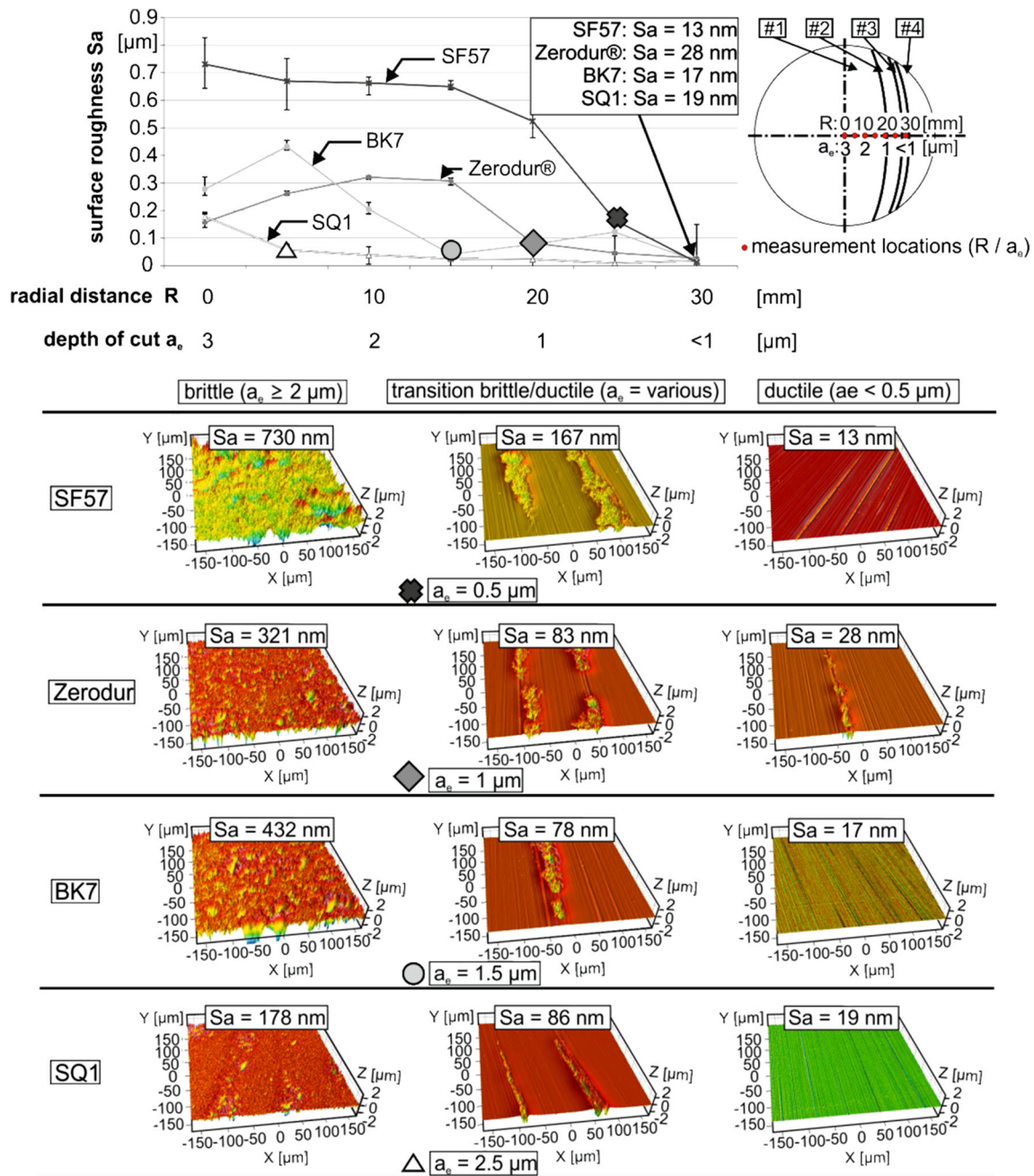


Fig. 9 Surface roughness and topographies of cross ground surfaces

$$t_{SSD} = T_{ca} - t_{ca} \tag{4}$$

$$T_{ca} = R_{ba} - \sqrt{R_{ba}^2 - \frac{D_{ca}^2}{4}} \tag{5}$$

$$t_{ca} = R_{ba} - \sqrt{R_{ba}^2 - \frac{d_{ca}^2}{4}} \tag{6}$$

By calculating the difference (Eq. 4) between the depth of the polished calotte (T_{ca} , calculated by Eq. 5) and the depth of the detected damage (t_{ca} , calculated by Eq. 6), the subsurface damage can be specified. Regarding Fig. 11, the

subsurface damage of the ground workpieces shows a similar performance as the surface roughness (Fig. 9). The lowest values of subsurface damage are detected for SQ1 (3 μm), followed by Zerodur® (6 μm) and BK7 (8 μm) at a distance of 30 mm to workpiece’s center point. SF57 generally reveals high values for subsurface damage, so that even in ductile machined areas the crack depth t_{SSD} is 21 μm, which is explainable by the low critical stress intensity factor ($0.75 \text{ MPam}^{1/2}$, next higher value is $0.9 \text{ MPam}^{1/2}$ for SQ1). Once the crack formation has started,

Fig. 10 Procedure for determination of subsurface damage of ground surfaces in cross grinding experiments

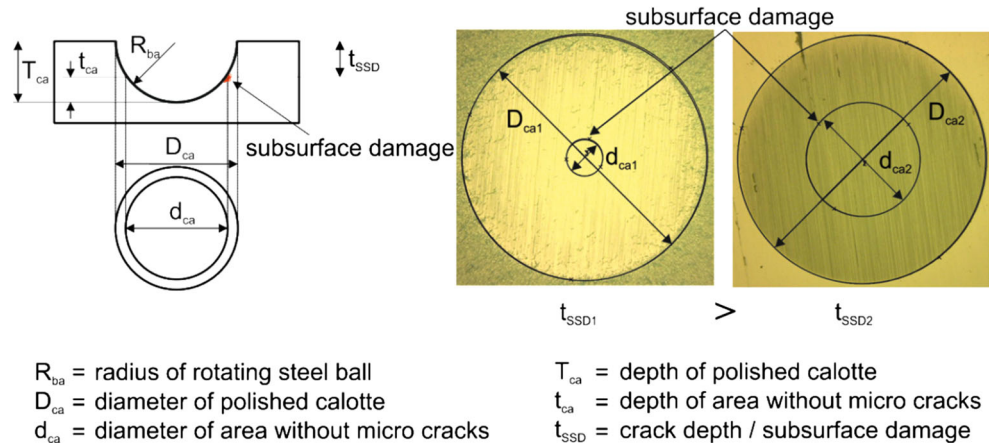
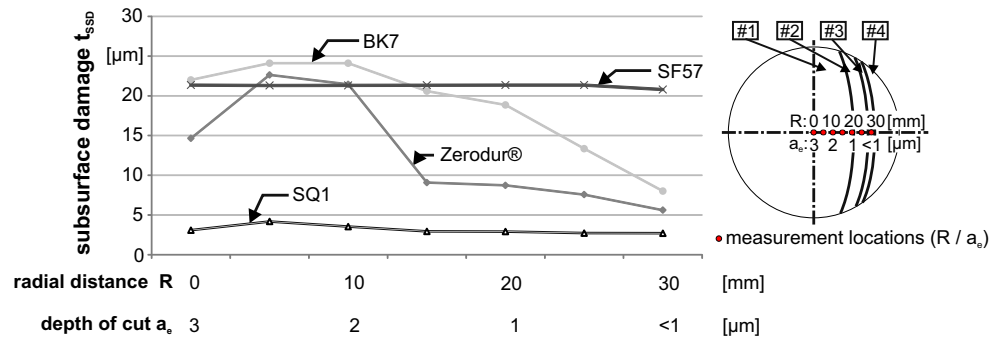


Fig. 11 Subsurface damage of ground surfaces in cross grinding experiments



which also happens at low depths of cut for SF57, it spreads quickly into the bulk material, leading to high subsurface damage. In brittle machined areas, the subsurface damage is too high for the detection mode presented here, because the calottes cannot be polished deep enough ($t_{SSD} > T_{ca}$). SQ1 shows a contrary behavior, as the subsurface damage is less than 5 μm, even for higher depths of cut.

4.3 Cross grinding of Zerodur® with constant depth of cut

Based on the results of the previously performed cross grinding experiments, optimized parameters are identified by the evaluation of the maximum chip thickness, taking the kinematical conditions in cross grinding into account (Table 5). With these parameters, a surface with a diameter of 50 mm is machined in Zerodur® with a constant depth of cut $a_e = 1 \mu\text{m}$.

Afterwards, the specimen has been investigated again by white light interferometry regarding surface roughness.

The values of surface roughness after grinding show that a predominant ductile machining of Zerodur® is possible with engineered grinding wheels within a radial distance of 25 mm. The measured Sa values are between 7 and 30 nm (Fig. 12). Still there are Sa-values larger than 20 nm,

Table 5 Optimized grinding parameters for cross grinding of Zerodur®

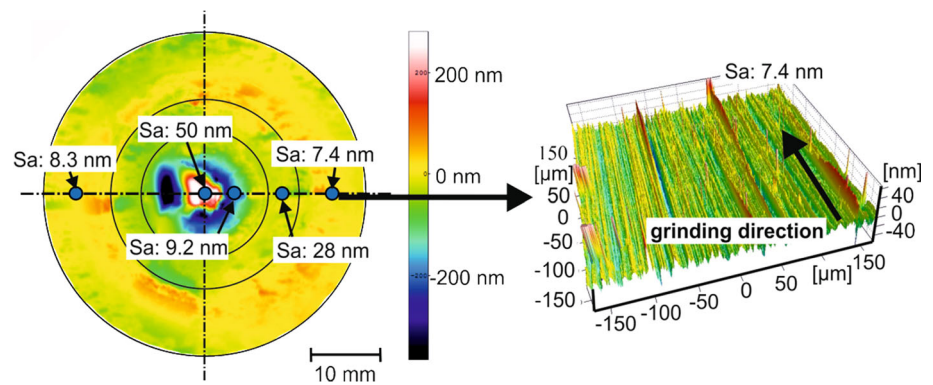
Workpiece materials	Zerodur®
Feed rate v_f (mm/min)	2
Cutting speed v_c (m/s)	30
Workpiece rotation n_w (min^{-1})	6
Depth of cut a_e (μm)	1

correlating with the results shown in cross grinding experiments with different depths of cut, which showed that particular brittle damage appears at a depth of cut $a_e = 1 \mu\text{m}$. Especially at the workpiece’s center, Sa values of 50 nm are measured due to kinematical effects, as the workpiece rotational speed approximates to zero, so that the material removal is not caused by a uniform chip formation (cutting), but more by cracking the material.

5 Conclusion and outlook

In this study, the machining of the optical materials SF57, Zerodur®, BK7 and SQ1 with coarse-grained engineered grinding wheels was performed. Plunge-cut surface grinding experiments with different depth of cut revealed the critical depth of cut at the transition point between brittle

Fig. 12 Interferometric measurement of the ground Zerodur[®] specimen and surface roughness values



and ductile machining. It could also be shown that engineered grinding wheels are applicable for ductile machining of these materials, but that all materials exhibit a quite low critical depth of cut ($<0.5 \mu\text{m}$). The reason for that is the fact that only a small amount of diamond grains (approx. 150 grains over the whole circumference of the grinding wheel of maximum 750 grains) are active during the grinding process. That means that only these grains are responsible for removing the material. Additionally, only a few of these grains cause the inserting brittle fracture. Nevertheless, ductile machining is possible due to the flattened grains and the consequential generation of a hydrostatic pressure in the contact zone. The second grinding kinematics was performed in order to proof the capability of engineered grinding wheels for grinding large surfaces with a predominant ductile mode. By tilting the workpiece, different depths of cut could be achieved like in plunge-cut surface grinding experiments. The results showed that the transition between brittle and ductile material removal takes place at different depths of cut for all materials. It must be taken into account that the machining process is not only influenced by the depth of cut, but also for the grinding kinematics, leading to differing maximum uncut chip thickness over the ground surface. Still it is possible to machine a homogeneous surface by setting a constant depth of cut, like grinding experiments on Zerodur[®] have shown. The surface revealed Sa values $\leq 50 \text{ nm}$ within an area of 2000 mm^2 .

In further grinding experiments, the material SQ1 will be ground, as it exhibited the best surface qualities in cross grinding experiments. Furthermore, the flattening of more diamond grains and the generation of a more uniform topography of the abrasive layer is pursued by advanced dressing technologies in order to activate more diamond grains for the grinding process.

Acknowledgments The authors would like to thank the German Research Foundation (Deutsche Forschungsgemeinschaft DFG) for funding the project “Engineered Grinding Wheels”—Deterministisches Präzisionsschleifen optischer Gläser (#BR 825/53-3).

References

- Brinksmeier E, Mutluguenes Y, Klocke F, Aurich JC, Shore P, Ohmori H (2010) Ultra-precision Grinding. *CIRP Ann Manuf Technol* 59:652–671. doi:10.1016/j.cirp.2010.05.001
- Bifano TG, Dow TA, Scattergood RO (1991) Ductile-regime grinding: a new technology for machining brittle materials. *Trans ASME J Eng Ind* 113:184–189
- Lawn BR, Jensen T, Aurora A (1976) Brittleness as an indentation size effect. *J Mater Sci Lett* 11:575
- Marshall DB, Lawn BR (1986) Indentation of Brittle Materials. *Microindentation Techniques in Materials Science and Engineering*, ASTM STP 889. In: Blau PJ, Lawn BR (eds) ASTM, Philadelphia, pp 26–46
- Biermann D, Wuerz E (2009) A study of grinding silicon nitride and cemented carbide materials with diamond grinding wheels. *Prod Eng Res Devel* 3(4):411–416. doi:10.1007/s11740-009-0183-z
- Rickens K, Grimme D, Riemer O, Brinksmeier E (2006) Engineered diamond wheels for precision ductile grinding. *Prod Eng Res Devel* 13(2):275–280
- Zhao Q (2015) Ultra-precision grinding of optical glasses using mono-layer nickel electroplated coarse-grained diamond wheels. Part 1: ELID assisted precision conditioning of grinding wheels. *Precis Eng* 39:56–66. doi:10.1016/j.precisioneng.2014.07.006
- Bing G, Zhao Q, Xiaoyan F (2014) Precision grinding of optical glass with laser micro-structured coarse-grained diamond wheels. *J Mater Process Technol* 214:1045–1051. doi:10.1016/j.jmatproc.2013.12.013
- Brinksmeier E, Mutluguenes Y, Riemer O (2013) Dressing of coarse grained diamond grinding wheels utilizing the thermo-chemical reaction. *Proc Euspen Int Conf* 2:125–128
- Marinescu ID, Hitchiner M, Uhlmann E, Rowe WB, Inasaki I (2007) *Handbook of machining with grinding wheels*. CRC Press, Boca Raton, pp 270–278
- Heinzel C, Rickens K (2009) Engineered wheels for grinding of optical glass. *Ann CIRP* 58(1):315–318. doi:10.1016/j.cirp.2009.03.096
- Zou L, Dong G, Zhou M (2013) Investigation on frictional wear of single crystal diamond against ferrous metals. *Int J Refract Metal Hard Mater* 41:174–179. doi:10.1016/j.jrmhm.2013.03.008
- Shimada S, Tanaka H, Higuchi M, Yamaguchi T, Honda S, Obata K (2004) Thermo-chemical wear mechanism of diamond tool in machining of ferrous metals. *Ann. CIRP* 53(1):57–60. doi:10.1016/S0007-8506(07)60644-1
- Brinksmeier E, Heinzel C, Rickens K, Althoff M, Berger D (2016) Präzisionsschleifen mit groben Diamantkörnern. *wt Werkstatttechnik* 6:387–393

15. Contardi C, Taylor ER, Fu A (2001) Study of UV-written channels in lead silicate glasses. *J Non-Cryst Solids* 291:113–120. doi:[10.1016/S0022-3093\(01\)00796-7](https://doi.org/10.1016/S0022-3093(01)00796-7)
16. Heiman D, Hamilton DS, Hellwarth RW (1979) Brillouin scattering measurements on optical glasses. *Phys Rev B (Condensed Matter)* 19(12):6583–6592
17. Scholze H (1988) *Glas. Natur, Struktur und Eigenschaften*. Springer, Berlin, p 213. ISBN 3-540-18977-7
18. Wray JH, Neu JT (1969) Refractive index of several glasses as a function of wavelength and temperature. *J Opt Soc Am* 59:774–776
19. Sun X, Stephenson DJ, Ohnishi O, Baldwin A (2006) An investigation into parallel and cross grinding of BK7 glass. *Prec Eng* 30:145–153. doi:[10.1016/j.precisioneng.2005.07.001](https://doi.org/10.1016/j.precisioneng.2005.07.001)